

Extracting latent variables from forecast ensembles and advancements in similarity metric utilizing optimal transport

Seiya Nishizawa¹

¹RIKEN Center for Computational Science

February 16, 2024

Abstract

This study presents a novel methodology for extracting latent variables from high-dimensional sparse data, particularly emphasizing spatial distributions such as precipitation distribution. This approach utilizes multidimensional scaling with a distance matrix derived from a new similarity metric, the Unbalanced Optimal Transport Score (UOTS). UOTS effectively captures discrepancies in spatial distributions while preserving physical units. This is similar to mean absolute error, however it considers location errors, providing a more robust measure crucial for understanding differences between observations, forecasts, and ensembles. Probability distribution estimation of these latent variables enhances the analytical utility, quantifying ensemble characteristics. The adaptability of the method to spatiotemporal data and its ability to handle errors suggest its potential as a promising tool for diverse research applications.

1 **Extracting latent variables from forecast ensembles and**
2 **advancements in similarity metric utilizing optimal**
3 **transport**

4 **S. Nishizawa¹**

5 ¹RIKEN Center for Computational Science

6 **Key Points:**

- 7 • Novel method reveals hidden information from spatial ensemble data for under-
8 standing probability distributions.
9 • Technique extracts essential similarities and differences in sparse distributions, aid-
10 ing interpretation for improved analysis.
11 • Approach is adaptable to different data types, making it promising for diverse sci-
12 entific fields.

Corresponding author: Seiya Nishizawa, s-nishizawa@riken.jp

13 **Abstract**

14 This study presents a novel methodology for extracting latent variables from high-dimensional
 15 sparse data, particularly emphasizing spatial distributions such as precipitation distri-
 16 bution. This approach utilizes multidimensional scaling with a distance matrix derived
 17 from a new similarity metric, the Unbalanced Optimal Transport Score (UOTS). UOTS
 18 effectively captures discrepancies in spatial distributions while preserving physical units.
 19 This is similar to mean absolute error, however it considers location errors, providing a
 20 more robust measure crucial for understanding differences between observations, fore-
 21 casts, and ensembles. Probability distribution estimation of these latent variables enhances
 22 the analytical utility, quantifying ensemble characteristics. The adaptability of the method
 23 to spatiotemporal data and its ability to handle errors suggest its potential as a promis-
 24 ing tool for diverse research applications.

25 **Plain Language Summary**

26 This study introduces a new method to understand weather patterns by simplifying
 27 complex data. A mathematical technique was developed to efficiently identify hid-
 28 den information from patterns. This assists meteorologists in understanding the weather
 29 with greater accuracy. This method simplifies weather data by highlighting the essen-
 30 tial similarities and differences between weather patterns, making it easier for scientists
 31 to interpret and use the resultant data effectively. This study offers a new and efficient
 32 way to make sense of vast weather data, benefiting meteorological research, and poten-
 33 tially improving weather forecasting. The technique contributes to the meteorological
 34 field, in addition it also contributes to various fields with sparse distribution data.

35 **1 Introduction**

36 Probabilistic forecasts play a pivotal role in systems characterized by chaotic or stochas-
 37 tic behavior, such as weather forecasting (Gneiting & Katzfuss, 2014). Ensemble sim-
 38 ulations are commonly employed to estimate the probability distributions of future states
 39 (Wilks, 2006). However, evaluating the predictive distribution in such multivariate, high-
 40 dimensional systems poses challenges, for instance in considering spatially distributed
 41 phenomena (Murphy, 1991).

42 While univariate cases allow straightforward distribution definitions based on en-
 43 semble member results, multivariate cases, particularly in high-dimensional systems such
 44 as weather forecasting, face the “curse of dimensionality” (Scott, 1992). Representing
 45 joint distribution that matches the state vector’s dimensionality becomes infeasible ow-
 46 ing to this issue, which influences accurate probability estimations.

47 Current discussions often focus on one-dimensional distributions, considering points
 48 individually (e.g., grid points) or single statistical quantities, such as spatial averages (Gneiting
 49 & Katzfuss, 2014). However, this point-wise approach could overlook crucial spatial pat-
 50 terns, especially in sparse quantities such as precipitation, leading to an overestimation
 51 of discrepancies between states, particularly in high-resolution simulation results (Gilleland
 52 et al., 2009).

53 This study tackles these limitations by leveraging the power of latent variables to
 54 capture the underlying structure and reduce complexity within high-dimensional ensem-
 55 ble data. Latent variables are hidden factors that influence observable data and repre-
 56 sent underlying structure and relationships in the data (Loehlin, 2004; Lee, 2007). The
 57 dimensionality of these latent variables can be significantly smaller than that of real vari-
 58 ables (for example, Turk & Pentland, 1991). This is supported by the fact that some sys-
 59 tems operate within small, embedded manifolds of lower dimensions, known as ranks (Foias
 60 et al., 1988; Constantin, 1989). By extracting these latent variables from ensemble sim-

61 ulations, I aim to create a lower-dimensional space that faithfully represents the essen-
62 tial features of the original data.

63 This study proposed a new novel methodological approach for extracting meaning-
64 ful latent variables from high-dimensional ensembles. Dimensionality reduction is a key
65 technique in this method to capture essential features and reduce the high-dimensional
66 ensemble data to more manageable data. The state vector obtained within the low-dimensional
67 space through dimension reduction serves as an estimate of the underlying latent vari-
68 ables. In the consideration of the probability distribution of ensemble data, the distance
69 between the ensemble members is important as it is intrinsic to the spread of the dis-
70 tribution. Therefore, to capture the essential characteristics of the probability distribu-
71 tion of ensemble data by reconstructing the probability distribution in a low-dimensional
72 latent variable space, a reduction method that preserves the distance is appropriate.

73 Several dimensionality reduction techniques exist. Principal component analysis
74 (PCA) is widely used for dimensionality reduction. However, it has limitations in non-
75 linear systems (for example, Nishizawa & Yoden, 2004) and is based on point-wise cal-
76 culation. The variational autoencoder (VAE; Kingma & Welling, 2013) can extract non-
77 linear relationships, and has received much attention in recent years, however, distance
78 information is lost due to normalization. It also faces challenges in predictive forecast
79 problems owing to limited ensemble sizes for training. In most practical cases, the en-
80 semble size is less than a hundred, and the size is insufficient to obtain latent variables
81 from the ensemble data by the VAE. Moreover, this approach requires previous knowl-
82 edge of the effective dimensions, which is the minimum number of dimensions of the la-
83 tent vectors necessary for a sufficiently accurate representation of the underlying phys-
84 ically meaningful structure of the original high-dimensional data. With some other di-
85 mension reduction methods, such as locally linear embedding (LLE; Roweis & Saul, 2000),
86 t-distributed stochastic neighbor embedding (t-SEN; Van der Maaten & Hinton, 2008),
87 uniform manifold approximation and projection (UMAP; McInnes et al., 2018), and densMAP
88 (Narayan et al., 2021), the distance is not maintained because low-dimensional variables
89 are reconstructed based on weights or probabilities corresponding to neighboring points.

90 In this study, multidimensional scaling (MDS; for example, Cox & Cox, 2000), specif-
91 ically classical MDS, a.k.a., principal coordinate analysis, is utilized to construct a Eu-
92 clidean low-dimensional space, where the distances between samples correspond to the
93 distance in the original high-dimensional state space. This method preserves the distance
94 in a dimension-reduced latent variable space and does not require prior knowledge of the
95 effective dimension of the system. MDS operates as a linear procedure. A nonlinear di-
96 mension reduction technique, Isomap (Tenenbaum et al., 2000), was also examined. Isomap
97 extends MDS by capturing nonlinear manifolds embedded within the original space. By
98 employing geodesic distance with a neighborhood graph, Isomap can be applied to com-
99 plex data structures beyond linear representations. The influence of the linear limita-
100 tion of MDS on the extracted state vectors was examined by employing Isomap.

101 The dimension reduction with MDS and Isomap is performed using a similarity met-
102 ric for all pairs of input samples. The units and magnitude of the similarity metric are
103 retained as a distance in the low-dimensional space. Therefore, the validity of the ex-
104 tracted latent variables significantly depends on the definition of the similarity metric
105 used, and the choice of an appropriate similarity metric is a critical aspect of this method.

106 To measure the similarity of two different states, several metrics exist. Existing met-
107 rics often fall short of capturing overall differences, leading to potentially misleading in-
108 terpretations. These metrics include traditional metrics, such as the mean absolute er-
109 ror (MAE), root mean squared error (RMSE), and Pearson correlation coefficient (CORR).
110 In addition, these include scores considering event-based dichotomous variables, such as
111 the frequency bias (FB, also called as bias ratio; for example, Wilks, 2006), equitable threat
112 score (ETS; Gilbert, 1884), and fractions skill score (FSS; N. M. Roberts & Lean, 2008;

113 N. Roberts, 2008). These were calculated point-wise, with the exception of FB and FSS.
 114 The point-wise comparison is known to double-penalize small-scale discrepancies (Gilleland
 115 et al., 2009). Among them, FSS is a score that allows some spatial displacement and is
 116 widely used for high-resolution simulations. However, as it is based on a categorized or
 117 thresholded quantity, it does not consider amplitude differences. When considering scores
 118 with different thresholds simultaneously to determine the event, the amplitude differ-
 119 ence may be implicitly interpreted. In cases with a large number of samples, the inter-
 120 pretation of multiple scores may require complex and difficult considerations. Recently,
 121 structure, amplitude and location (SAL; Wernli et al., 2008) and its extension for en-
 122 semble forecast (eSAL; Radanovics et al., 2018) have been used to evaluate validity of
 123 forecasts. However, they are not a single score but a combination of three independent
 124 scores corresponding to structure, amplitude and location errors. A comprehensive sin-
 125 gle score is preferred for several purposes, for example, estimating or characterizing a prob-
 126 ability distribution from ensemble. Therefore, FSS, SAL and eSAL are not suitable for
 127 the purposes like probability distribution estimation. The displacement and amplitude
 128 score (DAS; Keil & Craig, 2009) is a single score of combination of displacement and
 129 amplitude differences, containing more information than the traditional scores. However,
 130 there are several arbitrary in definitions and computational procedures. Keil and Craig
 131 (2007) showed that D_{\max} , which is the maximum search distance, has a great decisive
 132 impact on the result. It can only take discontinuous values: D_{\max} is proportional to grid
 133 spacing times a power of two. Therefore, it may be difficult to choose an appropriate value
 134 based on physical considerations owing to its discontinuous constraint. They suggested
 135 that other parameters had a minor impact, however, non-negligible arbitrariness which
 136 they did not discuss exists. The score was defined such that the amplitude difference be-
 137 tween one distribution and the morphed distribution of the other becomes the lowest;
 138 however, no condition was provided for the morphing flow, and in general, many possi-
 139 ble flows can achieve the smallest amplitude difference. Thus, there are many possi-
 140 bilities for displacement, and the total score depends on the displacement. Another ar-
 141 bitrary factor is the difference in weight between the displacement and amplitude. This
 142 score is a combination of these two differences. As they have different units, the differ-
 143 ences are normalized or nondimensionalized. On the original definition of DAS, the nor-
 144 malization factors are determined such that the two terms have equivalent weights. How-
 145 ever, there are other possibilities to choose the weights than the equivalent weights. In
 146 this sense, the weight parameter is inherently arbitrary. Indeed, there are arbitrary in
 147 the definition of the normalization factor of the amplitude error term I_0 . In addition,
 148 there is considerable arbitrariness in its computational procedure, resulting in a varia-
 149 tion in the score. In fact, this study’s implementation of computing the DAS results in
 150 a non-negligible difference in the obtained score compared to Keil and Craig (2009) for
 151 the same distributions owing to the undocumented details in the procedure. Another crit-
 152 ical issue is that the procedure does not consider mass conservation during morphing.

153 To address these issues in the existing metrics, this study introduces the Unbal-
 154 anced Optimal Transport Score (UOTS) as a novel similarity metric specifically designed
 155 for evaluating spatial distribution discrepancies. UOTS considers both amplitude and
 156 location differences in a unified manner, as does the DAS. However, the two terms of the
 157 displacement and amplitude differences have the same units and can be compared di-
 158 rectly. Therefore, nondimensionalization is not needed to combine them into a single score.
 159 UOTS is a more straightforward score that considers both displacement and amplitude
 160 differences than DAS. UOTS also has the same units as the original quantity, which fa-
 161 cilitates physical interpretations. UOTS offers significant advantages over existing met-
 162 rics by minimizing arbitrariness in its mathematical definition and providing clearer phys-
 163 ical interpretations, particularly regarding its hyperparameters.

164 The effectiveness of this approach and the suitability of UOTS in extracting mean-
 165 ingful latent vectors are demonstrated through experiments with synthetic and real-world
 166 meteorological data. This method is expected to provide valuable insight into high-dimensional

Table 1. Metrics for similarity used in this study. The rightmost column shows the conversion equation from the metric to the corresponding distance.

Abbreviation	Name	Distance
UOTS	Unbalanced optimal transport score	$UOTS$
DAS	Displacement and amplitude score	DAS
FSS	Fractions skill score	$1 - FSS$
MAE	Mean absolute error	MAE
RMSE	Root mean squared error	$RMSE$
CORR	Pearson correlation coefficient	$\sqrt{2(1 - CORR)}$
ETS	Equitable threat score	$1 - ETS$
FB	Frequency bias	$ \log(FB) $

167 ensemble data, leading to improved probability distribution estimation and ultimately,
 168 more accurate and informative forecasts.

169 2 Methods

170 2.1 Extracting Latent Variables

171 In this subsection, the proposed approach to extract latent variables from high-dimensional
 172 ensembles is described. The methodological approach was divided into two steps.

- 173 1. Calculation of a similarity metric for all pairs of ensemble members and observa-
 174 tions.
- 175 2. Extraction of latent variables in a low-dimensional space from the distance ma-
 176 trix based on the similarities.

177 2.1.1 Metric for Similarity

178 Assessing the similarity between spatial distributions requires a robust metric that
 179 capture various discrepancies, including amplitude, location, area, and shape differences.
 180 In this study, various metrics were employed to measure the similarity between spatial
 181 distributions. Table 1 summarizes the metrics used in this study.

182 *2.1.1.1 Unbalanced Optimal Transport Score* The UOTS proposed in this study
 183 serves as a novel similarity metric tailored to assess spatial distribution discrepancies.
 184 The UOTS is defined as follows:

$$185 \quad UOTS = \frac{1}{N} \min_{\gamma \in \mathbb{R}_{\geq 0}^{N^2}} \left[\left\{ 2 \sum_{i_1, i_2} \gamma_{i_1 i_2} \left(\frac{\|\mathbf{x}_{i_1} - \mathbf{x}_{i_2}\|_2}{L} \right)^q \right\} + \|\gamma \mathbf{1} - \phi_1\|_1 + \|\gamma^T \mathbf{1} - \phi_2\|_1 \right], \quad (1)$$

186 where \mathbf{x}_i represents the location of the point i , $\phi_1(\mathbf{x}_i)$ and $\phi_2(\mathbf{x}_i)$ are mass distribution
 187 in the two distributions which are to be compared. γ is the transport matrix, which is
 188 a $N \times N$ matrix whose element $\gamma_{i_1 i_2}$ is a non-negative real number representing the mass
 189 transported from \mathbf{x}_{i_1} to \mathbf{x}_{i_2} . $\mathbf{1}$ is a vector whose elements are all unity, and $\|\bullet\|_p$ rep-
 190 represents the L^p norm. The superscript T represents transposition. N is the vector length,
 191 i.e., $i = 1, \dots, N$. In this study, the score is defined as divided by N , however the num-
 192 ber of nonzero elements can be used instead of N , depending on the purpose.

193 The UOTS is defined based on optimal transport (OT), which is a mathematical
 194 problem introduced by Monge (1781). OT is an optimization problem of determining
 195 mass transport plan to minimize the overall cost of moving one mass distribution onto

196 another one with respected to given costs of moving a unit of mass between all pairs of
 197 spatial points. It has been widely used in various fields, especially in the machine learn-
 198 ing field, as a measure of similarity of non-negative distribution, such as probability dis-
 199 tributions. For OT, two distributions to be compared must have the identical mass; prob-
 200 ability density distributions have unit mass, however, spatial distributions, such as pre-
 201 cipitation distribution, can have various mass. Therefore, the OT cannot be used to mea-
 202 sure similarity for these distributions.

203 Unbalanced OT (UOT) is an extension of the OT to enable to apply to distribu-
 204 tions with different total mass. UOT has some variants in the form representing the mass
 205 difference. The most popular form is using Kullback–Leibler (KL) divergence (Kullback
 206 & Leibler, 1951) (Frogner et al., 2015). Another form is using L^1 norm, which is called
 207 the partial optimal transport (Caffarelli & McCann, 2010; Chizat et al., 2018; Figalli,
 208 2010), flat metric (Peyré & Cuturi, 2019), or Kantorovitch–Rubinshtain distance (Hanin,
 209 1992; Lellmann et al., 2014). UOTS is based on the UOT with L^1 form, normalized by
 210 the q -square of the length scale L . Thanks to the normalization, UOTS has the units
 211 of mass (or the units of the original quantity). In OT, the total mass is unity, or its value
 212 is usually normalized by the total mass, and thus the cost value has units of distance.
 213 Therefore, the optimal value in OT is often referred to as Wasserstein “distance”.

214 The OT and UOT have advantages over conventional metrics, such as point-wise
 215 norms and relative entropy, such as KL divergence, (Séjourné et al., 2023; De Plaen et
 216 al., 2023). One advantage is their ability to capture global structure, considering the over-
 217 all distribution and global relationship. They are sensitive to geometry and shapes, which
 218 an important feature as similarity metric. Another advantage is robustness to noise and
 219 outliers, as since they have information across the entire distribution, the impacts of in-
 220 dividual anomalies are reduced. Therefore, OT and especially UOT are less affected by
 221 noise and outliers, which are often contained in practical dataset.

222 UOTS inherits the advantages of OT and UOT. The UOTS captures both ampli-
 223 tude and location differences and is robust to noise and outliers. The UOTS employs the
 224 L^1 norm to express the mass difference as in the partial optimal transport, and can be
 225 interpreted as the mean absolute error when spatial displacements are considered. The
 226 first term in the brackets on the right-hand side of Eq. 1 penalizes mass transport or dis-
 227 placement of the distribution. $\gamma \mathbf{1}$ and $\gamma^T \mathbf{1}$ denote the transported source and target dis-
 228 tributions, respectively. Therefore, the second and third terms represent the mean ab-
 229 solute error after the transport. Through mass transport, the absolute error can be de-
 230 creased. On the other hand, larger transport costs more. The UOTS is to be determined
 231 to minimize the sum of the transport cost and the resulting absolute error, therefore, UOTS
 232 can be considered the mean absolute error with location error correction.

233 Its formulation involves the hyperparameters L and q . The parameter L determines
 234 the distance threshold for identifying same phenomena. Patterns exceeding this thresh-
 235 old are considered different. For the i_1 and i_2 index pairs, where $\|\mathbf{x}_{i_1} - \mathbf{x}_{i_2}\|_2 > L$, the
 236 optimized value of $\gamma_{i_1 i_2}$ must be zero; otherwise, the first term representing the trans-
 237 port cost outweighs the second and third terms representing the amplitude difference.
 238 To understand this, a simplest case of two points x_1 and x_2 can be considered, in which
 239 $\phi_1(x_1) > 0, \phi_2(x_2) > 0$, and $\phi_1(x_2) = \phi_2(x_1) = 0$. Then, it is evident that $\gamma_{12} \leq$
 240 $\min(\phi_1(x_1), \phi_2(x_2))$ and $\gamma_{11} = \gamma_{22} = \gamma_{21} = 0$. UOTS can be written as:

$$\begin{aligned}
 241 \quad UOTS &= \frac{1}{2} \min_{\gamma_{12} \in \mathbb{R}_{\geq 0}} \left\{ 2\gamma_{12} \left(\frac{\|\mathbf{x}_1 - \mathbf{x}_2\|_2}{L} \right)^q + (\gamma_{12} - \phi_1(x_1)) + (\gamma_{12} - \phi_2(x_2)) \right\} \\
 242 &= \frac{1}{2} \min_{\gamma_{12} \in \mathbb{R}_{\geq 0}} \left[2\gamma_{12} \left\{ \left(\frac{\|\mathbf{x}_1 - \mathbf{x}_2\|_2}{L} \right)^q - 1 \right\} + \phi_1(x_1) + \phi_2(x_2) \right]. \quad (2)
 \end{aligned}$$

243 Therefore, $\gamma_{12} = 0$ since $\left(\frac{\|\mathbf{x}_1 - \mathbf{x}_2\|_2}{L} \right)^q - 1 > 0$.

244 Next, the range of possible values for UOTS is considered. In general, the lower
 245 bound is zero but there is no upper bound. It is instructive to consider the limit values
 246 for L , as the limit values give a range of the possible values of UOTS. As L decreases,
 247 transportation costs increase and the UOTS approaches MAE:

$$248 \quad \lim_{L \rightarrow 0} UOTS = \frac{1}{N} (\|\phi_{\text{int}} - \phi_1\|_1 + \|\phi_{\text{int}} - \phi_2\|_1) = \frac{1}{N} \|\phi_1 - \phi_2\|_1, \quad (3)$$

249 where ϕ_{int} is the intersection of ϕ_1 and ϕ_2 . This is because $\gamma_{i_1 i_2}$ must be zero for $i_1 \neq$
 250 i_2 , for which $\|\mathbf{x}_{i_1} - \mathbf{x}_{i_2}\|_2 > 0$, otherwise the term representing transport cost becomes
 251 infinity. On the other hand, as L increases, transportation costs decrease and the UOTS
 252 approaches the mean mass difference, or bias:

$$253 \quad \lim_{L \rightarrow \infty} UOTS = \frac{1}{N} (\|\gamma \mathbf{1} - \phi_1\|_1 + \|\gamma^T \mathbf{1} - \phi_2\|_1) = \frac{1}{N} \left| \|\phi_1\|_1 - \|\phi_2\|_1 \right|, \quad (4)$$

254 because $\gamma^T \mathbf{1} = \phi_2$ and $\|\gamma \mathbf{1}\|_1 = \|\phi_2\|_1$, when $\|\phi_1\|_1 \geq \|\phi_2\|_1$; and vice versa. For in-
 255 termediate L , the UOTS have the value between the two limits (MAE and the mean mass
 256 difference) as $\frac{1}{N} \left| \|\phi_1\|_1 - \|\phi_2\|_1 \right| \leq UOTS \leq \frac{1}{N} \|\phi_1 - \phi_2\|_1$.

257 The other hyperparameter q affects the transportation cost per mass. The larger
 258 the value of q , the more the difference in position is disregarded and the more tolerant
 259 the score is for small displacement errors. This is because $\frac{\|\mathbf{x}_{i_1} - \mathbf{x}_{i_2}\|_2}{L} \leq 1$ where $\gamma_{i_1 i_2} >$
 260 0 .

261 In the actual computation in this study, the minimization problem for this opti-
 262 mization was solved by using the Sinkhorn algorithm (Cuturi, 2013) with a reservoir of
 263 dustbin points by incorporating a regularization term $\lambda \Omega(\gamma)$ as in ordinary partial op-
 264 timal transport. Here, Ω and λ represent the entropy regularization function and its co-
 265 efficient, respectively, and $\Omega(\gamma) = \sum_{i_1, i_2} \gamma_{i_1 i_2} \log(\gamma_{i_1 i_2})$. In this study, the parameter
 266 λ was fine-tuned to the smallest possible value without causing computational divergence.

267 The UOTS introduces a novel approach that comprehensively evaluates the simi-
 268 larity between spatial distribution patterns, while having a clear physical interpretation
 269 of its hyperparameters.

270 **2.1.2 Extraction of Latent Variables in Dimension-Reduced Space**

271 Before extracting the latent variables in a reduced space, a distance matrix was con-
 272 structed from the similarity metric between all pairs of the ensemble members and the
 273 observational data. In the process of constructing the distance matrix, it is crucial to
 274 transform metrics into values resembling distances that signify zero for identical distri-
 275 butions, nonnegatives, and symmetry, as detailed in Table 1.

276 **2.1.2.1 Multidimensional Scaling** MDS allows for the extraction of state vectors
 277 in Euclidean space while preserving the given distance. It also reveals the relative im-
 278 portance of each coordinate and the number of effective dimensions based on stress func-
 279 tions. The state vector in the space can be obtained by solving an eigendecomposition
 280 problem of the matrix $K = -\frac{1}{2} H D H$, where D is the distance matrix and H is the cen-
 281 tering matrix $H = I - \frac{1}{N} \mathbf{1} \mathbf{1}^T$, and I is the identity matrix. The vector \mathbf{v}_m correspond-
 282 ing the state of the m -th ensemble member is obtained such that its k -th element is $v_{km} =$
 283 $\sqrt{\lambda_k} u_{mk}$, where λ_k and u_{mk} are the k -th eigenvalue and the m -th element of the k -th
 284 eigenvector, respectively. Coordinates corresponding to larger eigenvalues are more prin-
 285 cipal. By considering only a small number of principal eigenvalues/eigenvectors (i.e., prin-
 286 cipal coordinates), a vector of smaller dimension can be obtained. It is noted that the
 287 result of the MDS is identical to PCA when the Euclidean distance, i.e., RMSE, in the
 288 original high-dimensional space is used as the similarity metric (Cox & Cox, 2000).

289 The stress function S is computed as follows:

$$290 \quad S = \sqrt{\frac{\sum_{m_1 < m_2} (\hat{d}_{m_1 m_2} - d_{m_1 m_2})^2}{\sum_{m_1 < m_2} \hat{d}_{m_1 m_2}}}, \quad (5)$$

291 where $\hat{d}_{m_1 m_2}$ represents the distance in the reduced space ($\hat{d}_{m_1 m_2} = \|\mathbf{v}_{m_1} - \mathbf{v}_{m_2}\|_2$),
 292 and $d_{m_1 m_2}$ is the distance derived from the similarity metric in the original space be-
 293 tween members m_1 and m_2 . The stress function changes value depending on how many
 294 dimensions of the \mathbf{v}_m are considered when calculating the distance \hat{d} . In other words,
 295 it is a function of the number of the dimensions δ .

296 2.2 Experiments

297 2.2.1 Synthetic Data Experiment

298 The synthetic data experiment was designed following the methodology detailed
 299 in Ahijevych et al. (2009) to illustrate the characteristics of various similarity metrics
 300 for assessing spatial distributions. A prescribed geometric spatial distribution mimick-
 301 ing the accumulated surface precipitation distribution was utilized. This distribution is
 302 described as follows:

$$303 \quad \phi(x, y) = \begin{cases} 0, & \left(\frac{x-x_1}{a}\right)^2 + \left(\frac{y-y_1}{b}\right)^2 \geq 1 \\ \Phi_1, & \left(\frac{x-x_1}{a}\right)^2 + \left(\frac{y-y_1}{b}\right)^2 < 1, \quad \left(\frac{x-x_2}{0.4a}\right)^2 + \left(\frac{y-y_1}{0.4b}\right)^2 \geq 1 \\ \Phi_2, & \left(\frac{x-x_2}{0.4a}\right)^2 + \left(\frac{y-y_1}{0.4b}\right)^2 < 1 \end{cases}, \quad (6)$$

304 where $x_2 = x_1 + 0.4a$, $\Phi_2 = 2\Phi_1$, and $x = i\Delta x$ and $y = j\Delta x$, with $i = 0, 1, \dots, 601$, $j =$
 305 $0, 1, \dots, 501$ and $\Delta x = 4$ km.

306 Six spatial distributions (Fig. 1) were created, including one reference (observa-
 307 tion) and five target patterns (forecasts). The parameters (x_1, a, b) for the reference, pat-
 308 tern 1, pattern 2, pattern 3, pattern 4, and pattern 5 are $(200\Delta x, 25\Delta x, 100\Delta x)$, $(250\Delta x, 25\Delta x, 100\Delta x)$,
 309 $(400\Delta x, 25\Delta x, 100\Delta x)$, $(325\Delta x, 100\Delta x, 100\Delta x)$, $(325\Delta x, 100\Delta x, 25\Delta x)$, and $(325\Delta x, 200\Delta x, 100\Delta x)$,
 310 respectively. In all distributions, $y_1 = 250\Delta x$ and $\Phi_1 = 12.7$ mm.

311 2.2.2 Synthetic Data Ensemble Experiment

312 Furthermore, in this study, the geometric distribution (Section 2.2.1) was extended
 313 to ensemble forecasts and multiple cases. The observations and ensemble members were
 314 generated using specific parameters to simulate diverse scenarios, resulting in 100 cases
 315 with 50 ensemble members each.

316 The parameters for the observations are $(x_1^{\text{obs}}, y_1^{\text{obs}}, a^{\text{obs}}, b^{\text{obs}}, \Phi_1^{\text{obs}}) = (300\Delta x, 250\Delta x, \sqrt{\frac{A}{\pi\alpha}}, \sqrt{\frac{A\alpha}{\pi}}, 2^{\epsilon_3/2})$,
 317 where A and α are the area and aspect ratios, respectively, and $(A, \alpha) = (2^{\epsilon_1/2}\pi a_0 b_0, 4^{\epsilon_2/2}\frac{b_0}{a_0})$.
 318 The constants were set as $a_0 = 25\Delta x$ and $b_0 = 100\Delta x$ based on the reference in the
 319 synthetic data experiment. ϵ_s are random numbers with a standard normal distribution.

320 The parameters for ensemble members are $(x_1^{\text{fcs}}, y_1^{\text{fcs}}, a^{\text{fcs}}, b^{\text{fcs}}, \Phi_1^{\text{fcs}}) = (x_1^{\text{obs}} + 50\Delta x\epsilon_4, y_1^{\text{obs}} +$
 321 $50\Delta x\epsilon_5, \sqrt{\frac{A^{\text{fcs}}}{\pi\alpha^{\text{fcs}}}}, \sqrt{\frac{A^{\text{fcs}}\alpha^{\text{fcs}}}{\pi}}, 2^{\epsilon_8/2}\Phi_1^{\text{obs}})$, where, $(A^{\text{fcs}}, \alpha^{\text{fcs}}) = (2^{\epsilon_6/2}A^{\text{obs}}, 4^{\epsilon_7/2}\alpha^{\text{obs}})$. Note
 322 that, for the location difference, i.e., $x_1^{\text{fcs}} - x_1^{\text{obs}}$ and $y_1^{\text{fcs}} - y_1^{\text{obs}}$, 95% of samples (corre-
 323 sponding to 2 standard deviations) statistically range from $-100\Delta x$ to $100\Delta x$. For the
 324 area, aspect ratio, and amplitude, the factors of $2^{\epsilon/2}$ and $4^{\epsilon/2}$ were set so that 95% of
 325 samples statistically ranged from 0.5 to 2, and 0.25 to 4, respectively.

326 2.2.3 Real Data Experiment

327 In order to examine applicability of the method to practical applications, real pre-
 328 cipitation data was used. The data had a spatial distribution of radar reflectivity at 2-

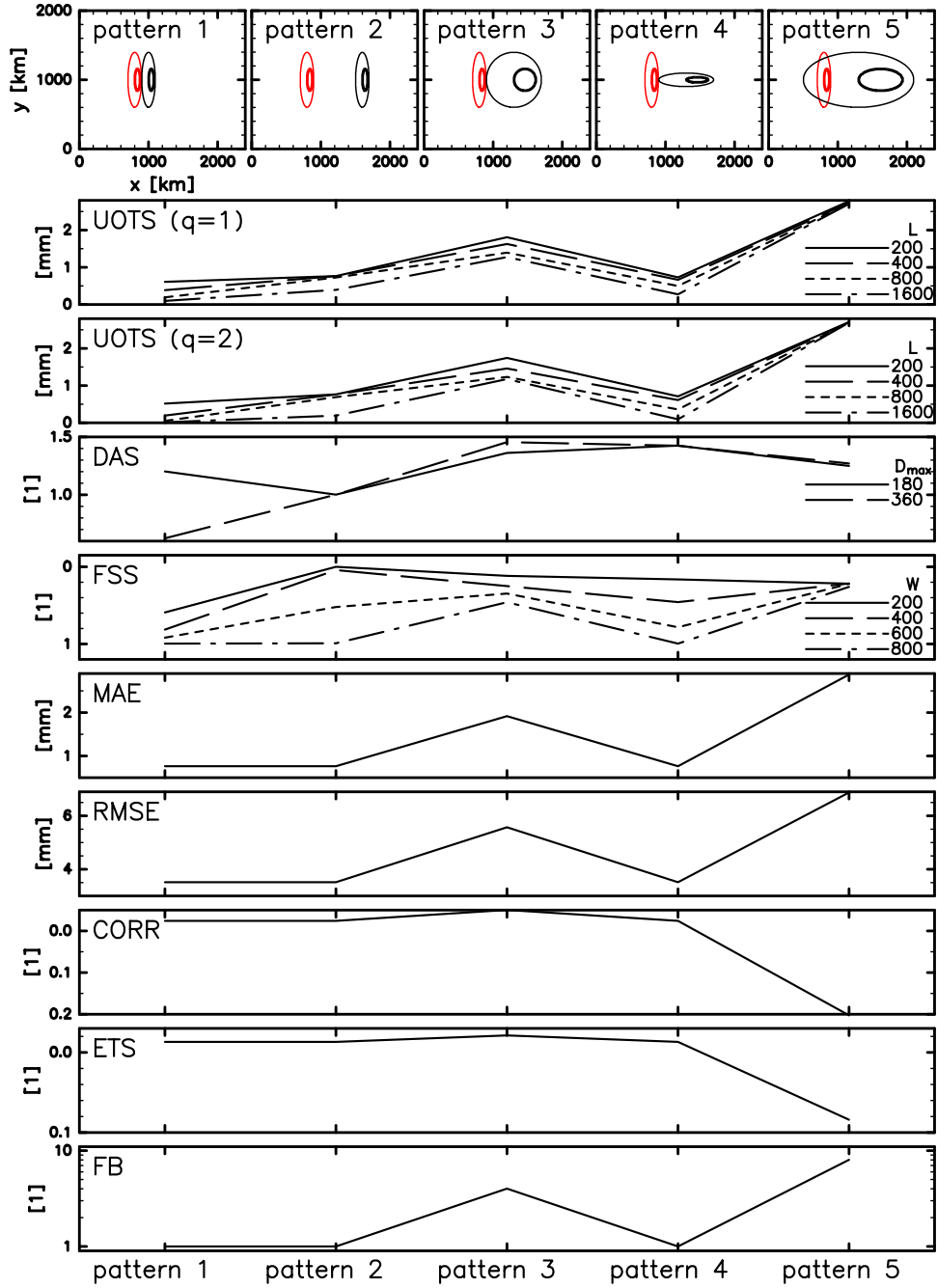


Figure 1. Spatial pattern of the geometric distributions in the synthetic data experiment. The top panels display the reference (observation) and five distributions (forecasts). The red and black color indicates observation and forecasts, respectively. The thin and thick contours represent the area at which $\phi = 12.7$ and 25.4 mm, respectively. The lower panels show the magnitude of similarity metrics for the five distributions with respect to the reference. The vertical coordinates are oriented such that the bottom (top) is more similar (more different). Solid, dashed, dotted, and dash-dotted lines indicate $L = 200, 400, 800,$ and $1,600$ km for UOTS, $W = 200, 400, 600,$ and 800 km for FSS, respectively. Solid and dashed lines indicate $D_{\max} = 180,$ and 360 km for DAS, respectively.

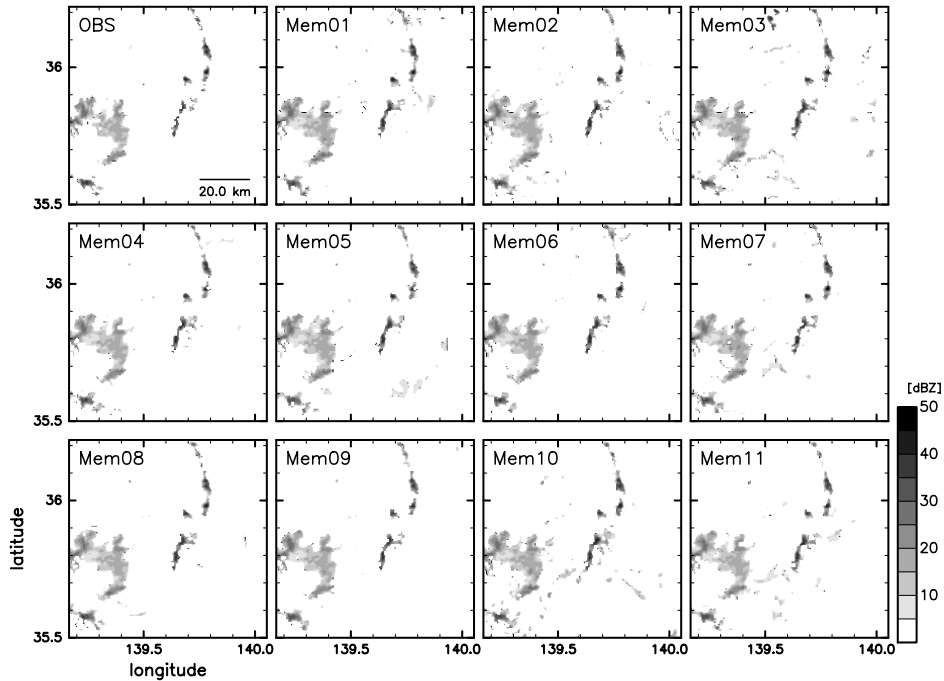


Figure 2. Longitude-latitude cross-section of the radar reflectivity in dBZ in the real data experiment. The top-left panel display the observation. The other panels are of 11 ensemble members out of 50 members.

329 km height at 18:00 UTC, 29 July 2021 obtained in Miyoshi et al. (2023). A real-time 30-
 330 second-refresh numerical weather prediction was conducted at Kanto region in Japan dur-
 331 ing Tokyo Olympics and Paralympics in 2021 using supercomputer Fugaku. In the pre-
 332 diction system, a regional atmospheric model SCALE-RM (Scalable Computing for Ad-
 333 vanced Library and Environment-Regional Model, Nishizawa et al., 2015; Y. Sato et al.,
 334 2015) and a data assimilation framework SCALE-LETKF (SCALE-local ensemble trans-
 335 form Kalman filter, Lien et al., 2017) was utilized and generated analysis data every 30
 336 seconds with 1,000 ensemble members of 500-m-mesh simulations assimilating 3-D vol-
 337 ume radar observations obtained by the phased array weather radar installed at Saitama
 338 University. In this study, data of 50 members out of the 1,000 members was used. The
 339 data covers about $80 \times 80 \text{ km}^2$ domain and its spatial resolution is 500 m (161×161
 340 grids). The smaller values less than 5 dBZ were rounded to zero.

341 Figure 2 shows the horizontal distribution of the radar reflectivity of the observa-
 342 tion and some of the ensemble members. The ensemble members have similar patterns
 343 to the observation with some differences.

344 3 Results

345 3.1 Synthetic Data Experiment

346 The characteristics of the various similarity metrics were examined using geomet-
 347 ric spatial distributions (Section 2.2.1). The experiment involved multiple metrics and
 348 the sweeping of their hyperparameters. L and q for UOTS were swept: $L = 200, 400,$
 349 $800,$ and $1,600$ km, and $q = 1$ and 2 . The FSS also had a hyperparameter W which rep-
 350 represents the width of neighborhoods, and it was swept for 200, 400, 600, and 800 km. The

351 parameters for DAS were set to $D_{\max} = 180$ and 360 km, and I_0 were set 15.4 mm ac-
 352 cording to previous research (Keil & Craig, 2009).

353 Figure 1 visually demonstrates the magnitude of various similarity metrics applied
 354 to the five target patterns (forecasts) with respect to the reference (observation). The
 355 difference of the forecast of the pattern 1 from the observation is obviously smaller than
 356 that of other patterns. However, the score for the pattern 1 is not the best with the DAS
 357 with $D_{\max} = 180$, CORR, and ETS. UOTS displayed consistent rankings across pat-
 358 terns, indicating lower sensitivity against parameter changes. Conversely, DAS and FSS
 359 exhibited higher sensitivity to their parameters, signifying the necessity for careful pa-
 360 rameter selection. Although the parameters L , W , and D_{\max} for the UOTS, FSS, and
 361 DAS, respectively, all indicate the limit distance for location difference, dependency of
 362 the scores on the parameter exhibits such significant difference. The lower sensitivity,
 363 or higher robustness, is a favorable trait to determine single value representing similar-
 364 ity. Traditional scores, such as RMSE, MAE, CORR, ETS, and FB, as previously re-
 365 ported by Ahijevych et al. (2009), showed limitations in distinguishing between patterns
 366 1, 2, and 4, i.e., different location and aspect-ratio errors. These outcomes emphasize the
 367 advantages of UOTS as a more robust similarity metric.

368 3.2 Synthetic Data Ensemble Experiment

369 To demonstrate the extraction of latent variables and advantages of the UOTS, a
 370 synthetic data ensemble experiment was conducted (Section 2.2.2). Figure 3 presents the
 371 distributions of the estimated latent variables in two-dimensional space with the two lead-
 372 ing coordinates. With the independent parameters given in the distribution generation,
 373 the two coordinates are anticipated to be independent if the latent variables are success-
 374 fully extracted. When utilizing UOTS, DAS, and FSS with a moderate W , the first and
 375 second coordinates appear to be independent. Conversely, in cases employing RMSE,
 376 MAE, ETS, CORR, FB, and FSS with small and large W , these two coordinates exhibit
 377 a relationship. The FB and FSS with a large W are nearly one-dimensional, relying solely
 378 on the first coordinate. FB and FSS with large W depend solely on the area difference
 379 and disregard other errors, leading to a one-dimensional latent variable distribution. The
 380 dependency on the parameter with UOTS is much lower than with FSS, which is con-
 381 sistent with the result in the previous experiment (Section 3.1). Despite the lower de-
 382 pendency, it is relatively larger with $q = 2$ than with $q = 1$. UOTS with $L = 1,600$
 383 and $q = 2$ shows a relatively one-dimensional structure, since UOTS depend solely on
 384 the area difference in the case of $L = \infty$. ETS, CORR, and FSS with small W were
 385 distributed in a two-dimensional space however exhibited a rather one-dimensional struc-
 386 ture. Reasons for this may be considered as follows: The metrics reach the upper bound
 387 value even with a low location error, and many pairs of the ensemble members tend to
 388 have the same value, i.e., the upper bound value. In fact, in the synthetic data exper-
 389 iment, these metrics have the value near the upper bound for most of the patterns (Fig.
 390 1). In the two-dimensional latent variable space, they try to locate to have an equal dis-
 391 tance, resulting the circular structure. The distributions using MAE and RMSE display
 392 intermediate characteristics between the two-dimensional independent structure (e.g.,
 393 with UOTS) and one-dimensional structure (e.g., ETS). Furthermore, as the ensemble
 394 members were generated by adding or multiplying a normal random number to the ob-
 395 servation parameters, the observation state was expected to be located near the origin
 396 in the latent variable space. With UOTS, FSS with a medium W , and FB, the obser-
 397 vation was located near the origin, as expected. However, the observations are not po-
 398 sitioned near the origin for the other cases. From this perspective, UOTS and FSS with
 399 medium W emerged as favorable similarity metrics among those investigated. Although
 400 Fig. 3 represents distributions in a single case, their qualitative characteristics described
 401 above are consistent across all the cases.

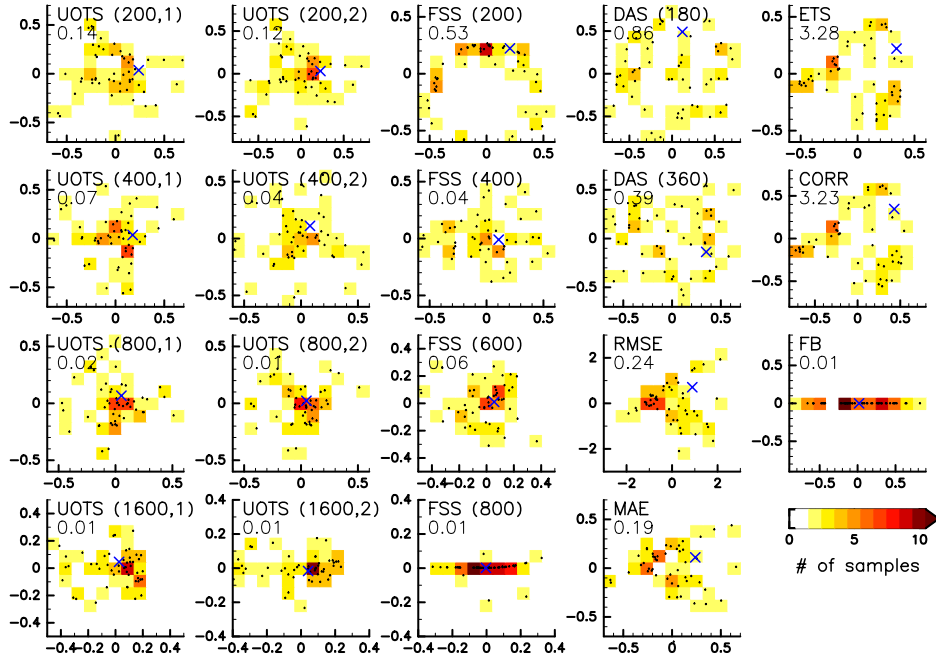


Figure 3. (Scatter plot) Locations of the individual ensemble member and observation in the leading two-dimensional latent variable space and (tone) their two-dimensional histograms. The black dots and blue x symbol indicate the ensemble member and observation, respectively. The numbers in parentheses represent L and q for UOTS, W for FSS, and D_{\max} for DAS. The number under the metric name is the mean distance of the observation from the origin in the two-dimensional space normalized by the standard deviation of the distance of ensemble members from the origin averaged over all the 100 cases.

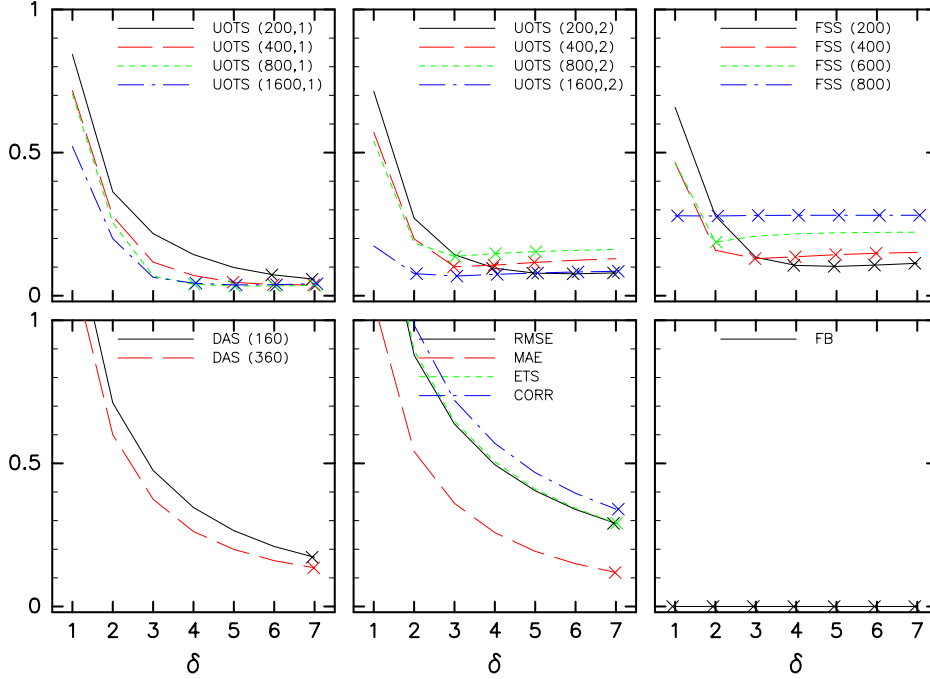


Figure 4. Dependency of the stress on the number of dimension δ . Different color and line types indicate different metrics and parameters. The number in parentheses represent L and q for UOTS, W for FSS, and D_{\max} for DAS. The x symbols indicate the dimension at which the stress is less than the minimum value plus 0.02.

402 In this experiment, the latent variable was expected to be five dimensions, since
 403 the distributions were generated with five independent parameters: the amplitude, two-
 404 dimensional location, area, and aspect ratio. The effective dimensionality of the estimated
 405 latent variables is explored using the stress function (Fig. 4). The effective dimension-
 406 ality is estimated as the dimension δ at which the stress becomes constant, i.e., minimum
 407 value: For example, when the effective dimension is five, the stress will decrease for $\delta \leq$
 408 5, and remain constant for $\delta \geq 5$. UOTS with $L = 400$ and $q = 1$ exhibited an effective
 409 dimensionality of five, aligned with the expectations. However, the effective dimension-
 410 ality depends on L : it is tend to be smaller as L becomes large. This tendency can
 411 be seen for both $q = 1$ and 2. This indicates that some information was being discarded
 412 for larger L , since UOTS solely depends on the area in the limit of $L \rightarrow \infty$. This in-
 413 formation loss is remarkable for the FSS with $W = 800$ and FB, and the stress was al-
 414 most constant for all δ , corresponding to a one-dimensional structure. On the other hand,
 415 some metrics displayed a continuous stress reduction even beyond five dimensions, sug-
 416 gesting an overestimation of dimensionality: UOTS with $L = 200$ and $q = 1$, DAS,
 417 RMSE, MAE, ETS, and CORR. With FSS of $W = 200$ and 400, it becomes constant
 418 at $\delta = 4$ and 3, respectively. The fact that FSS does not consider the amplitude error
 419 is related to this underestimation of the dimensionality. Conversely, the stress increases
 420 as δ increases with UOTS with $L = 400, 600, 800$ and $q = 2$, and FSS with $W = 600$.
 421 This implies that these metrics are not appropriate for representing the Euclidean dis-
 422 tance. These results suggests that a moderate L and $q = 1$ are suitable to obtain di-
 423 mensionality reasonably.

424 To investigate the relationship between the five given parameters (x, y, A, α and
 425 Φ) and the extracted coordinates, a correlation analysis was performed. In this exper-
 426 iment, if the latent variable is correctly extracted, information of all five parameters should
 427 be contained in the five leading coordinates. In each case, the correlation coefficients be-
 428 tween the parameters and the elements of the extracted vector corresponding to the five
 429 leading coordinates were computed. As the order of the leading coordinates can vary de-
 430 pending on the case, the highest correlation coefficient among the five leading coordi-
 431 nates was selected for each parameter in each case. Figure 5 displays the averaged cor-
 432 relation coefficient in all cases with error bars indicating the 99% confidence level for each
 433 parameter. The correlation coefficients for all five parameters were mostly higher than
 434 0.36 for UOTS with larger L s. The value of 0.36 is the threshold of the correlation co-
 435 efficient calculated with 50 samples to be statistically significant at the 99% significance
 436 level. For other metrics, some of the correlation coefficients are lower than the thresh-
 437 old, indicating that the extracted latent variables do not have information of some given
 438 parameters, that is, the metrics lost some information. This confirms that UOTS suc-
 439 cessfully extracted information of the five parameters.

440 Overall, UOTS with $L = 400\text{--}800$ and $q = 1$ emerged as the most preferred sim-
 441 ilarity metrics among those investigated, providing insights into the latent variable dis-
 442 tribution.

443 Furthermore, the linearity constraints inherited in MDS were considered. The dis-
 444 tributions in two-dimensional space displays a one-dimensional structure with ETS, CORR,
 445 and FSS with $W = 200$. This can be attributed to the limitations of linearity inher-
 446 ent to MDS. To address this limitation, the nonlinear method Isomap was employed. How-
 447 ever, the distributions in two-dimensional space obtained with Isomap are similar to those
 448 obtained using conventional MDS with ETS and CORR. For FSS with $W = 200$, al-
 449 though the shape changed significantly, it still exhibited a one-dimensional structure. This
 450 implies that the dimensionality constraint is inherent to the characteristics of the sim-
 451 ilarity metric. On the other hand, the obtained distributions with UOTS using Isomap
 452 are almost identical to that using MDS. Therefore, when UOTS is used as similarity met-
 453 ric, MDS can be used to extract latent variables.

454 3.3 Real Data Experiment

455 The synthetic data ensemble experiment in Section 3.2 considers distributions with
 456 a single nonzero area, i.e., single phenomena, and practical scenarios involving multiple
 457 nonzero areas may require further consideration of the effectiveness of UOTS and ap-
 458 propriate L values. Therefore, in addition to the synthetic data, real application data
 459 (Section 2.2.3) was used to examine the applicability of this method. In the real data
 460 experiment, we do not know information about the true latent variables. Therefore, in
 461 this experiment, consistency of characteristics and dependency on the metric and param-
 462 eters with those in the synthetic data ensemble experiment was considered.

463 As in the synthetic data ensemble experiment, the latent variables were extracted
 464 by the MDS with variety of similarity metrics. Figure 6 shows the spatial distributions
 465 of the extracted latent variables in the leading two-dimensional space. The character-
 466 istics are similar to those in the synthetic data ensemble experiment. As shown in the
 467 synthetic data ensemble experiment, it is almost one-dimensional with FB and FSS with
 468 large W . Sensitivity of the distribution on the parameter is much smaller with UOTS
 469 with $q = 1$ than with UOTS with $q = 2$ and FSS. As L becomes larger, the distribu-
 470 tion becomes nearly one-dimensional and this is more remarkable for $q = 2$. On the other
 471 hand, the one-dimensional structure seen with ETS, CORR, and FSS with small W in
 472 the synthetic data ensemble experiment is not clearly seen in the real data experiment.
 473 This may be because small-scale noises existing in the original data act as an spatial scat-
 474 ter or smoothing filter in the latent variable space.

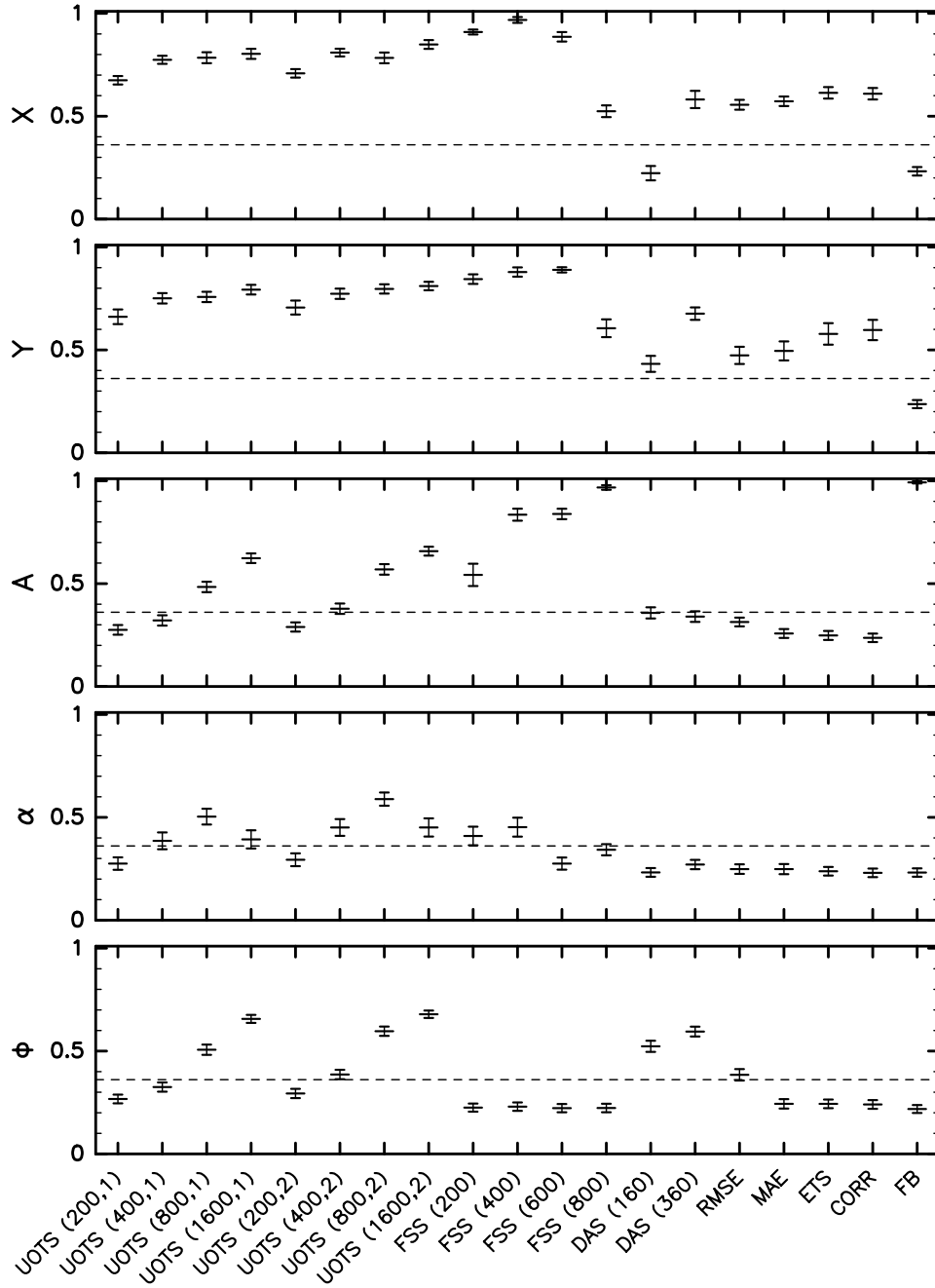


Figure 5. Correlation coefficient between the extracted latent variables and the prescribed five parameters, x, y, A, α and Φ , for each metrics averaged over the 100 cases in the synthetic data ensemble experiment. The error bar represents the 99% confidence interval. The dotted line shows the level above which the correlation calculated from 50 samples is statistically significant at 99% significance level.

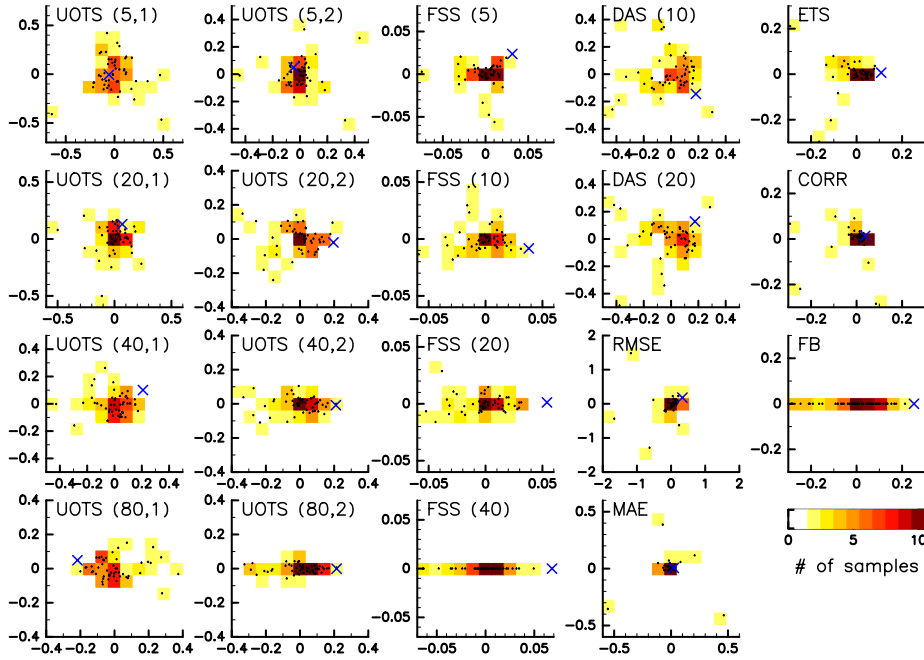


Figure 6. The same figure as Fig. 3 but in the real data experiment.

475 The dependency of the stress on the dimensionality also shows similar character-
 476 istics to the synthetic data ensemble experiment (Fig. 7). The sensitivity of the stress
 477 on the parameter is much smaller with UOTS with $q = 1$ than with UOTS with $q =$
 478 2 and FSS. Although the true value of the dimensionality is unknown in this experiment,
 479 UOTS with $q = 1$ shows that the effective dimensionality is about 10. The stress show
 480 continuous reduction with UOTS with $L = 5$ and $q = 2$, DAS, RMSE, MAE, ETS,
 481 and CORR. It increases for large δ with FSS with $W = 10, 20$ and 40. It is almost con-
 482 stant with FB and FSS with $W = 5$.

483 These consistency of the results support the advantages of UOTS and also suggest
 484 that UOTS can be applied to practical data.

485 4 Conclusions

486 This study proposes a novel methodology for extracting meaningful latent variables
 487 in low-dimensional space from high-dimensional, sparse data, primarily focusing on spa-
 488 tial distributions. The application of multidimensional scaling with a new similarity met-
 489 ric, namely, the UOTS, proves highly effective in achieving this goal. UOTS offers sev-
 490 eral advantages over traditional metrics, including incorporating amplitude and location
 491 errors and preserving physical meaning within its latent variables.

492 The estimation of probability distributions from these latent variables using den-
 493 sity estimation methods, such as histogram or kernel density estimation, offers substan-
 494 tial analytical advantages over the original high-dimensional space. This approach of-
 495 fers several potential advantages for various applications. For example, it enables the de-
 496 termination of the ensemble mean and spread while considering crucial factors such as
 497 location differences, which are vital in numerous meteorological applications. The en-
 498 semble mean can be determined as the barycenter using the unbalanced optimal trans-

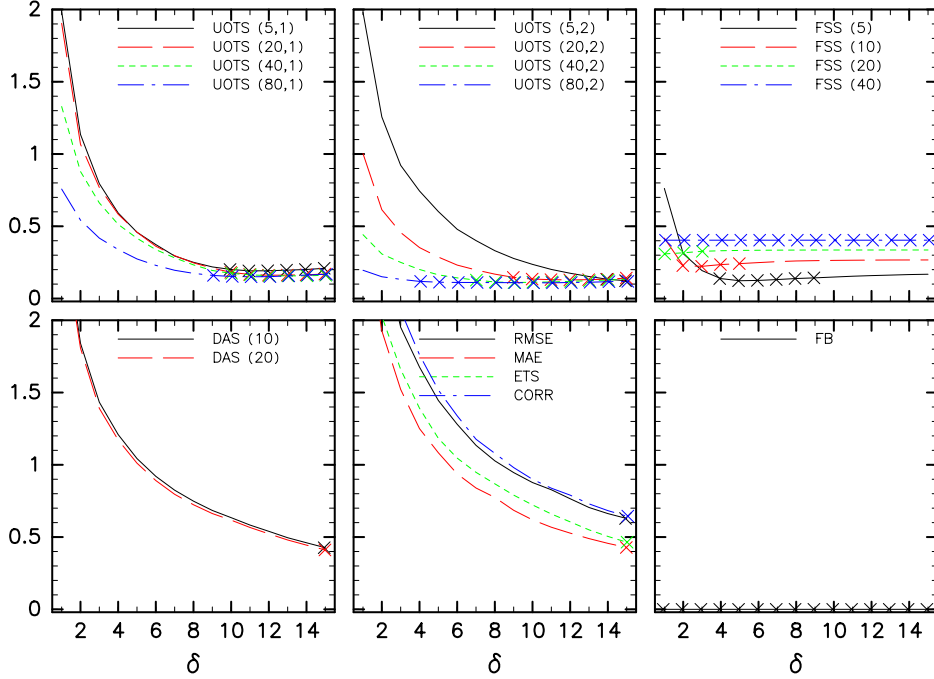


Figure 7. The same figure as Fig. 4 in for the real data experiment.

499 port theory, whereas the ensemble spread can be derived from the square root of the sum
 500 of the eigenvalues obtained by multidimensional scaling. To evaluate the probability dis-
 501 tribution and compare distributions in different cases, it is crucial that the Euclidean dis-
 502 tance in the latent variable space closely matches the distance in the original high-dimensional
 503 space. The UOTS has the same units as the original physical quantity and MDS pre-
 504 serves the units. Therefore, the method using the UOTS and MDS is preferable to con-
 505 sider the probability distribution in low-dimensional space.

506 The efficacy of this methodology is underscored by its ability to handle discrepan-
 507 cies in spatial distributions by considering the amplitude, location, area, and shape er-
 508 rors. However, the UOTS has two hyperparameters L and q and the efficacy of UOTS
 509 depends on these parameters. Therefore, determination of these parameters is one of the
 510 challenges of UOTS. Too small L waken the ability to collect the location error, since
 511 transport is allowed only within distance of L . On the other hand, too large L makes
 512 the score less sensitive to location errors and also creates the danger of equating differ-
 513 ent phenomena that are far apart. In the limit where L goes to zero and infinity, UOTS
 514 is equal to the MAE and the mean mass difference, respectively, and loses its advantages.
 515 The synthetic and real-data experiments suggest that a moderate L (around 400 km and
 516 20–40 km in the synthetic data ensemble and real data experiments, respectively) and
 517 $q = 1$ lead to the most informative latent variable distribution. Magnitude of the pa-
 518 rameter could be guessed based on physical properties of the phenomena of interest such
 519 as the spatial extent and typical distance of different phenomena. In the synthetic data
 520 ensemble experiment, the standard deviation of center position difference of two ensemble
 521 members is 400 km, since the variance of difference in x_1^{fcs} and y_1^{fcs} is $2(50\Delta x)^2$ and
 522 $\Delta x = 4$ km. This is almost same scale with the estimated appropriate value of L . In
 523 the real data experiment, typical spatial scale of the distribution of the reflectivity (Fig.
 524 2) is estimated to roughly be 10–20 km. From this physical scale, an appropriate L is
 525 estimated around 20 km. This is consistent the result of the sweep experiment. These

526 support the validity of choosing L based on the characteristics of physical phenomena
527 of interest.

528 With $q=1$, the UOTS is linearly related to the distance between two patterns to
529 be compared, i.e., the location error. This implies that the UOTS with $q=1$ has simi-
530 lar characteristics to that of the Euclidean distance and would be better matched for the
531 MDS.

532 Despite of these intuitive consideration, sweep experiment of these parameters may
533 be required to determine the appropriate value in practical cases as well as other simi-
534 larity metrics having hyperparameters, such as FSS. However, the number of trials for
535 the sweep can be much smaller for UOTS than that for FSS and DAS because of less
536 sensitivity of UOTS to the parameter. Even though the parameters of L , W , and D_{\max}
537 all indicate distance limit for location error or displacement, this smaller sensitivity, in
538 other word stronger robustness, is a preferable feature of UOTS in terms of parameter
539 determination. Furthermore, in the parameter sweep of L , the result of MAE and the
540 mean mass difference may give a hint because they are the limit of the UOTS as L goes
541 to zero and infinity.

542 One limitation of UOTS is its computational cost compared to conventional met-
543 rics. UOTS is obtained by iterative solver, thus the computation time highly depends
544 on input data and parameters. On average, the computation time for the UOTS in the
545 synthetic data experiment was about 5.3 seconds, while it is about 0.06 seconds for FSS
546 on my standard Intel CPU workstation. However, active research in optimal transport
547 is developing faster algorithms (for example, R. Sato et al., 2020). In addition, these al-
548 gorithms are know to be suitable for graphics processing unit computers. Therefore, these
549 promise future improvement in computational cost of UOTS.

550 Although the primary focus of this study was on the spatial distributions, this method
551 readily adapts to spatiotemporal distributions with minimal modifications. Incorporat-
552 ing factors, such as advection speed in the temporal direction, into the transport cost
553 of UOTS allows for a seamless extension while maintaining the core methodology.

554 The versatility of this approach extends to various meteorological applications, for
555 example, comparison of spatial distribution of aerosol and chemical species emitted from
556 specific locations such as Y. Sato et al. (2018). Moreover, this approach is not limited
557 to meteorology and it is also applicable to various fields dealing with sparse spatiotem-
558 poral distributions beyond meteorology. Its adaptability to diverse domains and robust-
559 ness in handling errors makes it a promising tool across scientific disciplines.

560 Acknowledgments

561 The author appreciates the associated editor and three reviewers for their efforts and valu-
562 able comments. This work was supported by JST [Moonshot R&D Program] Grant Num-
563 ber [JPMJMS2286]. The diagrams in this study were drawn using tools developed by
564 the GFD-Dennou Club (<http://www.gfd-dennou.org/>).

565 Open Research Section

566 The programs for analysis visualization, and input and output data used in this
567 study are available at Nishizawa (2024).

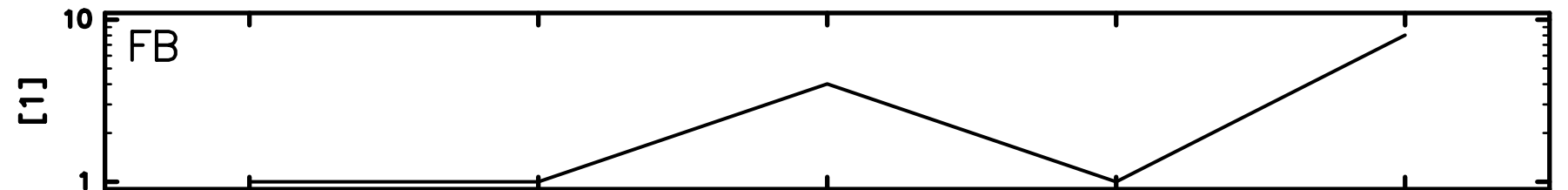
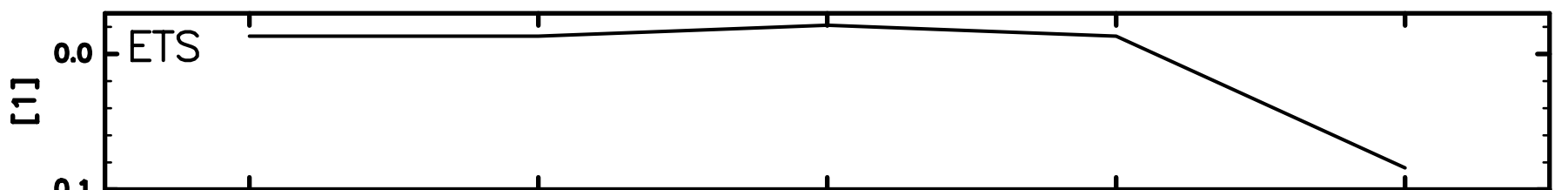
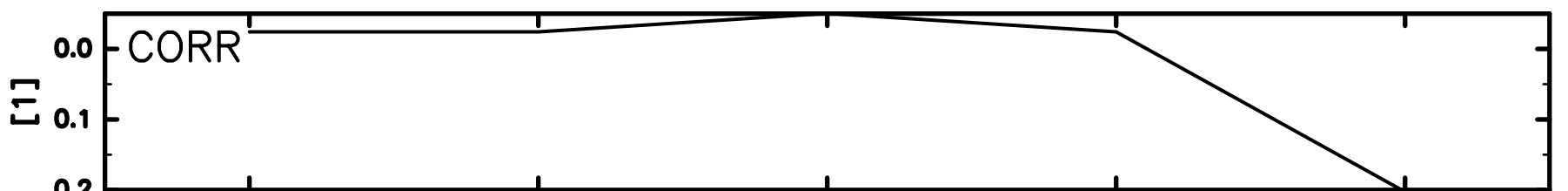
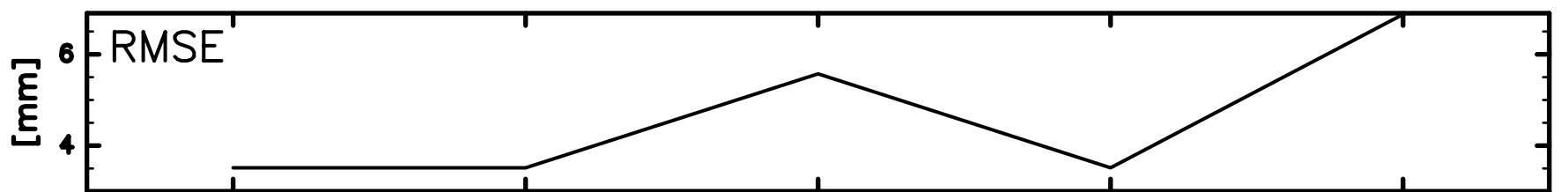
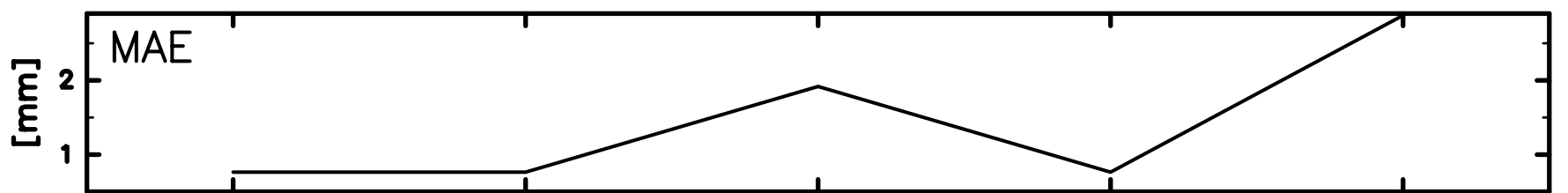
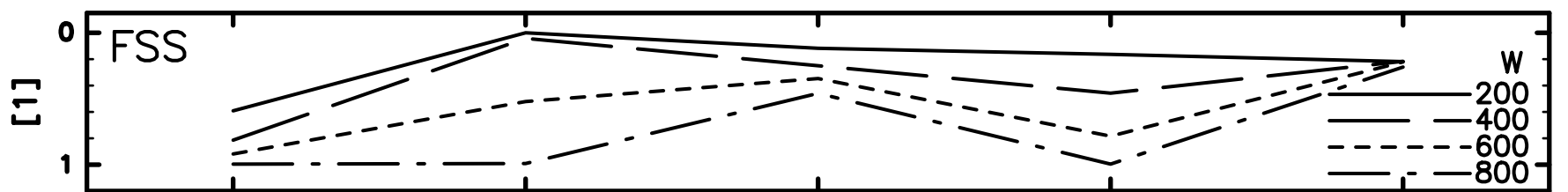
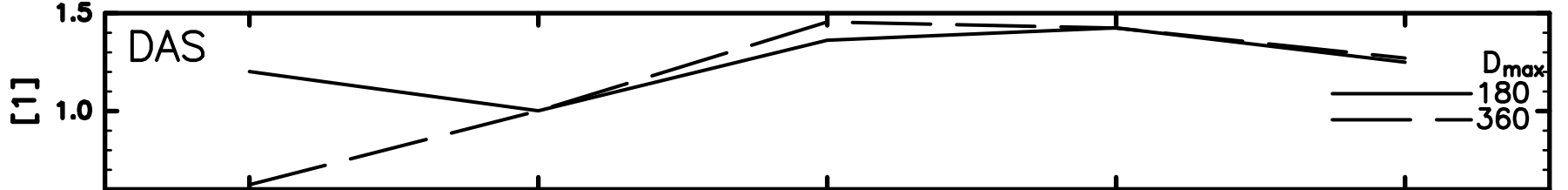
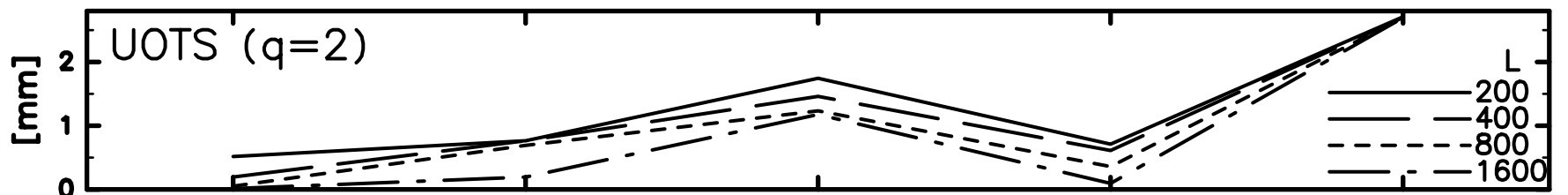
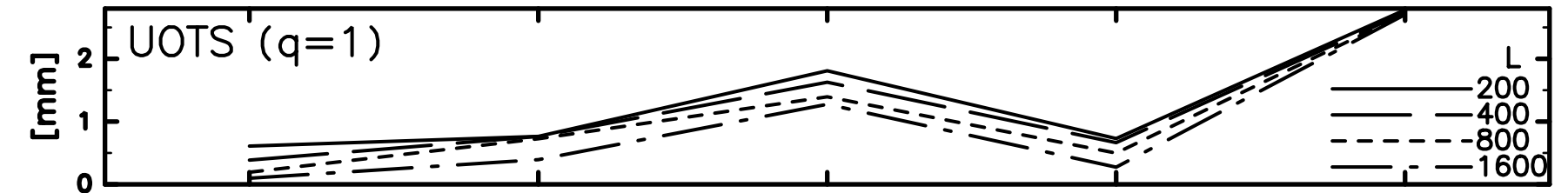
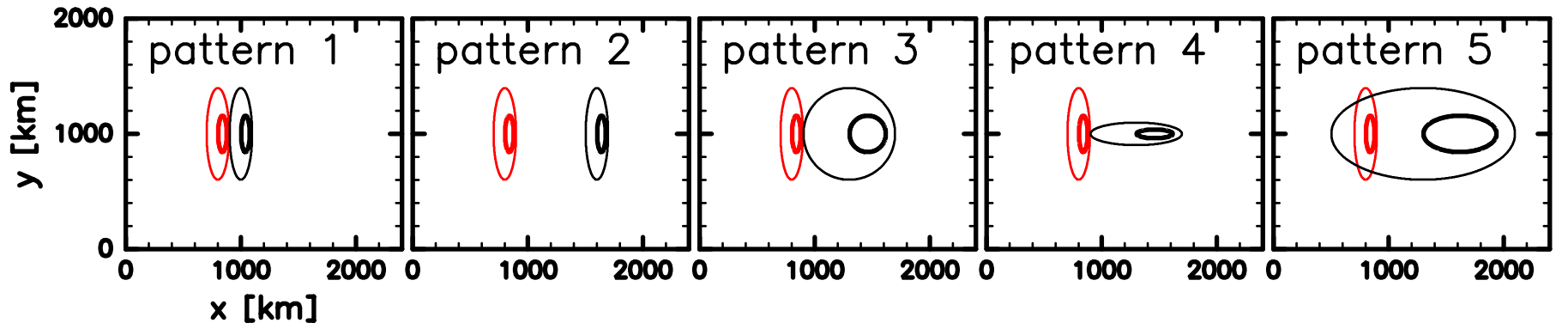
568 References

569 Ahijevych, D., Gilleland, E., Brown, B. G., & Ebert, E. E. (2009). Applica-
570 tion of spatial verification methods to idealized and NWP-gridded pre-
571 cipitation forecasts. *Weather and Forecasting*, 24(6), 1485–1497. doi:

- 572 10.1175/2009WAF2222298.1
- 573 Caffarelli, L. A., & McCann, R. J. (2010). Free boundaries in optimal transport and
574 Monge–Ampère obstacle problems. *Annals of mathematics*, 673–730.
- 575 Chizat, L., Peyré, G., Schmitzer, B., & Vialard, F.-X. (2018). Scaling algorithms
576 for unbalanced optimal transport problems. *Mathematics of Computation*,
577 87(314), 2563–2609. doi: 10.1090/mcom/3303
- 578 Constantin, P. (1989). *Integral manifolds and inertial manifolds for dissipative par-*
579 *tial differential equations* (Vol. 70). Springer Science & Business Media.
- 580 Cox, T. F., & Cox, M. A. (2000). *Multidimensional scaling*. CRC press.
- 581 Cuturi, M. (2013). Sinkhorn distances: Lightspeed computation of optimal trans-
582 port. In C. Burges, L. Bottou, M. Welling, Z. Ghahramani, & K. Weinberger
583 (Eds.), *Advances in neural information processing systems* (Vol. 26). Curran
584 Associates, Inc.
- 585 De Plaen, H., De Plaen, P.-F., Suykens, J. A. K., Proesmans, M., Tuytelaars, T.,
586 & Van Gool, L. (2023). Unbalanced optimal transport: A unified framework
587 for object detection. In *Proceedings of the IEEE/CVF conference on computer*
588 *vision and pattern recognition (CVPR)* (pp. 3198–3207).
- 589 Figalli, A. (2010). The optimal partial transport problem. *Archive for rational me-*
590 *chanics and analysis*, 195(2), 533–560. doi: 10.1007/s00205-008-0212-7
- 591 Foias, C., Sell, G. R., & Temam, R. (1988). Inertial manifolds for nonlinear evolu-
592 tionary equations. *Journal of differential equations*, 73(2), 309–353. doi: 10
593 .1016/0022-0396(88)90110-6
- 594 Frogner, C., Zhang, C., Mobahi, H., Araya, M., & Poggio, T. A. (2015). Learning
595 with a Wasserstein loss. *Advances in neural information processing systems*,
596 28.
- 597 Gilbert, G. K. (1884). Finley’s tornado predictions. *American Meteorological Jour-*
598 *nal.*, 1(5), 166.
- 599 Gilleland, E., Ahijevych, D., Brown, B. G., Casati, B., & Ebert, E. E. (2009). Inter-
600 comparison of spatial forecast verification methods. *Weather and forecasting*,
601 24(5), 1416–1430. doi: 10.1175/2009WAF2222269.1
- 602 Gneiting, T., & Katzfuss, M. (2014). Probabilistic forecasting. *Annual Review*
603 *of Statistics and Its Application*, 1, 125–151. doi: 10.1146/annurev-statistics
604 -062713-085831
- 605 Hanin, L. G. (1992). Kantorovich–Rubinstein norm and its application in the theory
606 of Lipschitz spaces. *Proceedings of the American Mathematical Society*, 115(2),
607 345–352. doi: 10.1090/S0002-9939-1992-1097344-5
- 608 Keil, C., & Craig, G. C. (2007). A displacement-based error measure applied in a
609 regional ensemble forecasting system. *Monthly Weather Review*, 135(9), 3248–
610 3259. doi: 10.1175/MWR3457.1
- 611 Keil, C., & Craig, G. C. (2009). A displacement and amplitude score employing an
612 optical flow technique. *Weather and Forecasting*, 24(5), 1297–1308. doi: 10
613 .1175/2009WAF2222247.1
- 614 Kingma, D. P., & Welling, M. (2013). Auto-encoding variational bayes. *arXiv*
615 *preprint arXiv:1312.6114*. doi: 10.48550/arXiv.1312.6114
- 616 Kullback, S., & Leibler, R. A. (1951). On information and sufficiency. *The annals of*
617 *mathematical statistics*, 22(1), 79–86.
- 618 Lee, S.-Y. (2007). *Handbook of latent variable and related models*. Elsevier. doi: 10
619 .1016/B978-0-444-52044-9.X5000-9
- 620 Lellmann, J., Lorenz, D. A., Schonlieb, C., & Valkonen, T. (2014). Imaging with
621 Kantorovich–Rubinstein discrepancy. *SIAM Journal on Imaging Sciences*,
622 7(4), 2833–2859. doi: 10.1137/140975528
- 623 Lien, G.-Y., Miyoshi, T., Nishizawa, S., Yoshida, R., Yashiro, H., Adachi, S. A.,
624 ... Tomita, H. (2017). The near-real-time SCALE-LETKF system: A case
625 of the September 2015 Kanto–Tohoku heavy rainfall. *Sola*, 13, 1–6. doi:
626 10.2151/sola.2017-001

- 627 Loehlin, J. C. (2004). *Latent variable models: An introduction to factor, path, and*
628 *structural equation analysis*. Psychology Press. doi: 10.4324/9781410609823
- 629 McInnes, L., Healy, J., & Melville, J. (2018). Umap: Uniform manifold approxima-
630 tion and projection for dimension reduction. *arXiv preprint arXiv:1802.03426*.
631 doi: 10.48550/arXiv.1802.03426
- 632 Miyoshi, T., Amemiya, A., Otsuka, S., Maejima, Y., Taylor, J., Honda, T., . . . Uno,
633 A. (2023). Big data assimilation: Real-time 30-second-refresh heavy rain fore-
634 cast using Fugaku during Tokyo Olympics and Paralympics. In *Proceedings*
635 *of the international conference for high performance computing, networking,*
636 *storage and analysis* (pp. 1–10). Association for Computing Machinery. doi:
637 10.1145/3581784.3627047
- 638 Monge, G. (1781). Mémoire sur la théorie des déblais et des remblais. *Mem. Math.*
639 *Phys. Acad. Royale Sci.*, 666–704.
- 640 Murphy, A. H. (1991). Forecast verification: Its complexity and dimensionality.
641 *Monthly Weather Review*, 119(7), 1590–1601. doi: 10.1175/1520-0493(1991)
642 119(1590:FVICAD)2.0.CO;2
- 643 Narayan, A., Berger, B., & Cho, H. (2021). Assessing single-cell transcriptomic
644 variability through density-preserving data visualization. *Nature biotechnology*,
645 39(6), 765–774. doi: 10.1038/s41587-020-00801-7
- 646 Nishizawa, S. (2024). *Programs and data used for extracting latent variables from*
647 *forecast ensembles and advancements in similarity metric utilizing optimal*
648 *transport [DataSet]*. Zenodo. <https://doi.org/10.5281/zenodo.10628522>.
- 649 Nishizawa, S., Yashiro, H., Sato, Y., Miyamoto, Y., & Tomita, H. (2015). Influ-
650 ence of grid aspect ratio on planetary boundary layer turbulence in large-
651 eddy simulations. *Geoscientific Model Development*, 8(10), 3393–3419. doi:
652 10.5194/gmd-8-3393-2015
- 653 Nishizawa, S., & Yoden, S. (2004). A parameter sweep experiment on topographic
654 effects on the annular variability. *Journal of the Meteorological Society of*
655 *Japan. Ser. II*, 82(3), 879–893. doi: 10.2151/jmsj.2004.879
- 656 Peyré, G., & Cuturi, M. (2019). Computational optimal transport: With applica-
657 tions to data science. *Foundations and Trends® in Machine Learning*, 11(5-
658 6), 355–607. doi: 10.1561/22000000073
- 659 Radanovics, S., Vidal, J.-P., & Sauquet, E. (2018). Spatial verification of ensemble
660 precipitation: an ensemble version of SAL. *Weather and Forecasting*, 33(4),
661 1001–1020. doi: 10.1175/WAF-D-17-0162.1
- 662 Roberts, N. (2008). Assessing the spatial and temporal variation in the skill of pre-
663 cipitation forecasts from an NWP model. *Meteorological Applications*, 15(1),
664 163–169. doi: 10.1002/met.57
- 665 Roberts, N. M., & Lean, H. W. (2008). Scale-selective verification of rainfall accu-
666 mulations from high-resolution forecasts of convective events. *Monthly Weather*
667 *Review*, 136(1), 78–97. doi: 10.1175/2007MWR2123.1
- 668 Roweis, S. T., & Saul, L. K. (2000). Nonlinear dimensionality reduction by locally
669 linear embedding. *science*, 290(5500), 2323–2326. doi: 10.1126/science.290
670 .5500.2323
- 671 Sato, R., Yamada, M., & Kashima, H. (2020). Fast unbalanced optimal transport on
672 a tree. *Advances in neural information processing systems*, 33, 19039–19051.
- 673 Sato, Y., Nishizawa, S., Yashiro, H., Miyamoto, Y., Kajikawa, Y., & Tomita,
674 H. (2015). Impacts of cloud microphysics on trade wind cumulus: which
675 cloud microphysics processes contribute to the diversity in a large eddy
676 simulation? *Progress in Earth and Planetary Science*, 2, 1–16. doi:
677 10.1186/s40645-015-0053-6
- 678 Sato, Y., Takigawa, M., Sekiyama, T. T., Kajino, M., Terada, H., Nagai, H., . . .
679 Nakajima, T. (2018). Model intercomparison of atmospheric ¹³⁷Cs from the
680 Fukushima Daiichi nuclear power plant accident: Simulations based on iden-
681 tical input data. *Journal of Geophysical Research: Atmospheres*, 123(20),

- 682 11–748. doi: 10.1029/2018JD029144
- 683 Scott, D. W. (1992). The curse of dimensionality and dimension reduction. In *Multi-*
684 *variate density estimation* (p. 195–217). John Wiley & Sons, Ltd. doi: 10.1002/
685 9780470316849.ch7
- 686 Séjourné, T., Peyré, G., & Vialard, F.-X. (2023). Unbalanced optimal transport,
687 from theory to numerics. In E. Trélat & E. Zuazua (Eds.), *Numerical control:*
688 *Part b* (Vol. 24, pp. 407–471). Elsevier. doi: 10.1016/bs.hna.2022.11.003
- 689 Tenenbaum, J. B., Silva, V. d., & Langford, J. C. (2000). A global geometric frame-
690 work for nonlinear dimensionality reduction. *Science*, *290*(5500), 2319–2323.
691 doi: 10.1126/science.290.5500.2319
- 692 Turk, M., & Pentland, A. (1991). Eigenfaces for recognition. *Journal of cognitive*
693 *neuroscience*, *3*(1), 71–86. doi: 10.1162/jocn.1991.3.1.71
- 694 Van der Maaten, L., & Hinton, G. (2008). Visualizing data using t-SNE. *Journal of*
695 *machine learning research*, *9*, 2579–2605.
- 696 Wernli, H., Paulat, M., Hagen, M., & Frei, C. (2008). SAL—a novel quality measure
697 for the verification of quantitative precipitation forecasts. *Monthly Weather*
698 *Review*, *136*(11), 4470–4487. doi: 10.1175/2008MWR2415.1
- 699 Wilks, D. S. (2006). *Statistical methods in the atmospheric sciences* (Vol. 91). Aca-
700 demic press.



pattern 1 pattern 2 pattern 3 pattern 4 pattern 5

